KOM
CORROSION AND MATERIAL PROTECTION JOURNAL
ORIGINAL ARTICLE
sciendo

Using green corrosion inhibitor to reduce maintenance cost for carbon steel saline water storage systems in the oil industry

Namus R. M.[1], Abass M. H.[2], Alali M.[3], Zedin N. K.[4]
[1] Mechanical Engineering department, Faculty of Engineering, Wasit University, Kut, Iraq
[2] Midland Oil Company, Iraqi Ministry of Oil, Iraq
[3] Department of Materials Engineering, Faculty of Engineering, University of Kufa, Najaf, Iraq.
[4] Department of Production Engineering & Metallurgy, University of Technology, Baghdad, Iraq
E-mail: mowahid.alali@uokufa.edu.iq

Carbon steel has long been used in storing the saline water that results from oil washing in the oil industry. However, a high corrosion rate is reported, resulting in significant economic losses for oil companies. In the Middle East oil field, the temperature touches 50ºC in Summer, causing increasing in corrosion rate for saline water steel storage tanks and pipes. In the present work, abundantly available wheat straw was used to prepare a cost-effective silicate inhibitor. The high inhibition efficiency of up to 94 % decreased the corrosion rate from severe corrosion for no-inhibitor specimen to close to low corrosion category for optimum inhibitor concentration specimen. The mechanism of the inhibition effect is the formation of a chemically adsorbed layer on the steel surface, which is successfully described by Langmuir isotherm. Additionally, at high concentrations of nano-silica, complex aggregates might form and be physically adsorbed on the surface of steel above the chemically adsorbed nano-silicate monolayer.

INTRODUCTION

Carbon steel has long been used as a key material in producing industrial equipment such as piping systems, cooling towers, and storage tanks because it possesses an excellent combination of high strength, low cost, and exceptional weldability [1]. However, carbon steel is prone to severe corrosion when exposed to corrosive fluids, including acidic solutions and saline water, resulting in high economic losses [2]. Crude oil is washed in desalters by water to remove salts, resulting in a huge amount of saline water, which is transported and stored to be treated later and reused. ASTM A106 Grade B pipe steel is commonly used in making pipelines and storage tanks that are used for the transportation and storage of saline water in the oil industry. In the above-mentioned process, water salinity is high, with total dissolved solids (TDS) reaching 35 ppt. At such a high level of salinity, the water is removed from the system and replaced with fresh water. Furthermore, in the Iraqi oil industry, the temperature in summer touches 50 °C, which increases corrosion rates in tanks and pipelines. The replacement cost of the damaged parts exceeds 100k American dollars per saline water storing system annually. Thus, protection against corrosion is crucially important. Using corrosion inhibitors is one of the most efficient and cost-effective ways to enhance corrosion resistance. Despite their effectiveness, synthetic corrosion inhibitors are infrequently used because of their high operating cost and negative environmental impacts [3]. Consequently, many researchers have been looking for eco-friendly corrosion inhibitors over the past few years [4]. Recently, new corrosion inhibitors have been extracted from various plant wastes. These natural corrosion inhibitors are costly affordable, readily available, relatively simple to produce and environmentally friendly [5]. Silicate has been employed as a corrosion inhibitor; it performs as an anodic inhibitor and forms a thin protective layer on the metal surface [6]. Furthermore, silicate-based corrosion inhibitors are expected to be costly affordable, non-toxic, and ecologically benign than existing inorganic corrosion inhibitors, such as lead and chromate-based inhibitors [7]. Wheat straw, a viable resource for silica production, is a byproduct of wheat milling processes and a major agricultural waste product [8]. Silica obtained from natural resources such as wheat straw has been the subject of research in various fields. The effect of silica and nano-silica on anticorrosion performance has shown successful [9], [10].

The present work aims to investigate the inhibition effect of nano-silicate solution extracted from wheat straw on the corrosion behaviour of ASTM A106 Grade B pipe steel used in the saline water storage system in the oil industry. Potentiodynamic polarization and Electrochemical Impedance Spectroscopy (EIS) were employed to study the inhibition mechanism.

Tab. 1 Chemical composition of ASTM A106 Grade B

Elements	C	Mn	P	S	Si	Cr	Mo	Ni	Fe
Chemical composition	0.22	1.01	0.021	0.024	0.07	0.01	0.03	0.1	Bal.

EXPERIMENTAL

Materials

The chemical composition of ASTM A106 steel Grade B is shown in Table 1. The material was supplied in a 3 mm thick plate and was sectioned in 15 mm diameter cylindrical samples via EDM. The samples were mechanically ground and polished in the traditional way, ending with 1 μm SilcoTM to have mirror-like surfaces with minimum residual surface damage.

Inhibitor preparations

Nano-silica extraction

The Iraqi Wheat Straw (WS) was used as a silica source to produce high-purity nanosilica particles by chemical precipitation methods. For preparation, row WS was washed with distilled water ten times to remove the dust and soluble particles, followed by drying in air at room temperature for 24 hours. 30 g of the washed WS was soaked in 250 mL of 3 mol/L HCl solution at 80°C for 4 hours; then, the mixture refluxed in the same acid at room temperature for 12 hours. The resultant WS mixture was washed with deionized water and filtered ten times to raise the pH to 7. The leached WS was burned at 750°C in a muffle furnace for 5 h to remove carbonaceous materials, then left to cool down. The resultant white powder is called wheat straw ash WSA.

Pure nano-silicate was extracted by treating twenty grams of WSA with 160 ml of 2.5 mol/L NaOH solution. The samples were stirred via a magnetic stirrer at 70 °C for 3 hours. Na_2SiO_3 was filtered through Whatman (No. 41 ashless) filter paper. The obtained solution Na_2SiO_3 is revealed in the below equation.

$$SiO_2 + 2NaOH \rightarrow Na_2SiO_3 + H_2O$$

The residue solution was carefully washed with 100 mL of boiling water. Then sulphuric acid 2.5 mol/L H_2SO_4 was added to precipitate the silicate solution in the form of white gelatinous solid SiO_2 by the gelation process:

$$Na_2SiO_3 + H_2SO_4 \rightarrow SiO_2 + Na_2SO_4 + H_2O$$

Finally, the white gelatinous solid SiO_2 was washed with worn deionized water and dried at 70°C for 3 h. The process resulted in white nano-silicate powder. More details about nano-silica extraction and characterization can be found elsewhere [11], [12].

Corrosion inhibitor preparation

1.2 g of prepared nano-silica powder was dissolved in 100 ml of 3 mol/L NaOH to produce a sodium nano-silicate solution according to the following equation:

$$(2NaOH)_{aq} + (SiO_2)_{powder} \rightarrow Na_2SiO_2 + H_2O$$

The mixture was agitated via a magnetic stirrer for an hour, forming a cloudy solution that was left overnight for stabilization and became clear.

Testing solution

35 g of NaCl was dissolved in 1 L of deionized water to prepare saline water. The inhibitor was added to the testing solution with different nano-silicate concentrations named 10, 20, 40, and 80 ppm.

Corrosion investigation

The surfaces were electrochemically characterized using a standard three-electrode corrosion cell with a saturated calomel electrode (SCE) as reference electrode (its potential vs SHE is 0.242 V), two graphitic rods as counter electrodes, and the material under testing as working electrodes. The volume of the cell was 600 mL, and the temperature of all tests was 55°C.

OCP and Potentiodynamic

As part of the test, samples were immersed in the solution with the assigned temperature and inhibitor concentration for half an hour, during which the open circuit potential (OCP) was recorded, followed by conducting Tafel tests for ± 0.25 V vs OCP at 0.5 mV/s scan rate for all samples. By using EZware-2013 software, corrosion parameters such as corrosion current density (i_{corr}), corrosion potential (E_{corr}) and anodic and cathodic slopes (β_a, β_c) were determined. All Tafel tests were repeated twice on different samples and showed good reproducibility.

Electrochemical impedance spectroscopy EIS

An Electrochemical Workstation CorrTest (CorrTest, China) was used to perform the EIS. All the EIS tests were performed after half an hour of sample immersion in the solution at the assigned temperature and inhibitor concentration. Ten points were measured per decade with a perturbation amplitude of 10 mV and a frequency range of 100 kHz to 15 mHz. Using ZView software, the data

was modelled with an appropriate electric equivalent circuit (EEC). The tests were repeated twice on different samples with good reproducibility.

RESULTS

OCP

Fig. 1 shows open circuit potential (OCP) as a function of time for ASTM A106 Grade B steel immersed in saline water at 55°C with and without adding naturally extracted inhibitor. In all shown cases, OCP sharply started decreasing at the beginning of the test, followed by a plateau. For a specimen without adding inhibitor, the OCP plateau started after 900 s at -0.488 V vs SCE. However, the time needed for OCP stabilization when adding the inhibitor decreased to less than 250 s for all inhibited specimens. Additionally, OCP stabilized at about -0.4 V vs SCE for 10 ppm and 20 ppm specimens and at less than -0.34 V vs SCE for 40 ppm and 80 ppm specimens. Adding the naturally extracted nano-silicate inhibitor clearly shifts OCP for ASTM A106 Grade B steel in saline water at 55°C toward more noble potential and decreases the time needed for OCP stabilization.

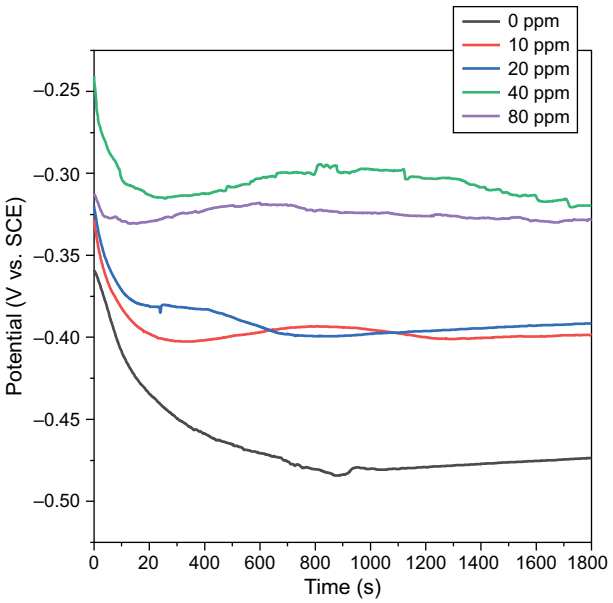


Fig. 1. OCP as a function of time for ASTM A106 Grade B steel in saline water at 55 °C with and without adding nano--silicate inhibitor

Potentiodynamic investigation

Fig. 2 shows the Tafel curves for ASTM A106 Grade B steel immersed in saline water at 55°C with and without adding naturally extracted inhibitor. The corrosion parameters were extracted and tabulated in Tab. 2. The apparent shifting of the E_{corr} toward anodic potential might suggest that the used inhibitor works as an anodic inhibitor [13], [14]; adding a nano-silicate inhibitor decreases the dissolution of ASTM A106 Grade B steel in saline water at 55 °C. Adding 10 ppm of the inhibitor to saline water caused decreasing in i_{corr} by more than half. Moreover, i_{corr} exhibits more decrease with further natural inhibitor being added to saline water; note that i_{corr} is one order of magnitude less when adding 80 ppm nano-silicate inhibitor to saline water compared to that when there is no inhibitor added. The inhibition efficiency IE_{tafel} (%) is determined based on i_{corr} using the following equation:

$$IE_{\text{Tafel}}\ \% = \frac{i^{0}_{\text{corr}} - i^{\text{inh}}_{\text{corr}}}{i^{0}_{\text{corr}}} \qquad (1)$$

where i^{0}_{corr} and i^{inh}_{corr} are the corrosion current densities in the absence and presence of the inhibitor. The significant enhancement in corrosion behaviour of ASTM A106 Grade B steel immersed in saline water at 55°C with adding nano-silicate solution inhibitor is apparently associated with increasing inhibition efficiency to ultimately reach 94% when 80 ppm of the inhibitor was added (Tab. 2 and Fig. 3).

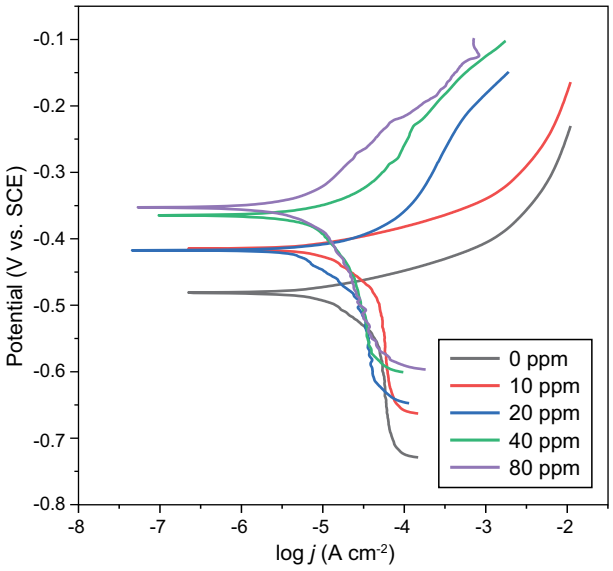


Fig. 2. Tafel plots for ASTM A106 Grade B steel in saline water at 55 °C with and without adding nano-silicate inhibitor

Tab. 2 Corrosion parameters derived from Tafel plots for ASTM A106 Grade B steel in saline water at 55 °C with and without adding nano-silicate inhibitor

Sample	E_{corr} (V)	i_{corr} (A cm^{-2}) × 10^{-5}	β_a (mV)	β_c (mV)	CR (mm/y)	IE_{Tafel} (%)
0 ppm	–0.48	4.23 ± 0.08	55	1056	0.49	–
10 ppm	–0.43	1.92 ± 0.10	79	492	0.226	46
20 ppm	–0.41	1.44 ± 0.06	106	432	0.17	67
40 ppm	–0.35	0.63 ± 0.02	120	191	0.076	85
80 ppm	–0.32	0.27 ± 0.01	89	137	0.031	94

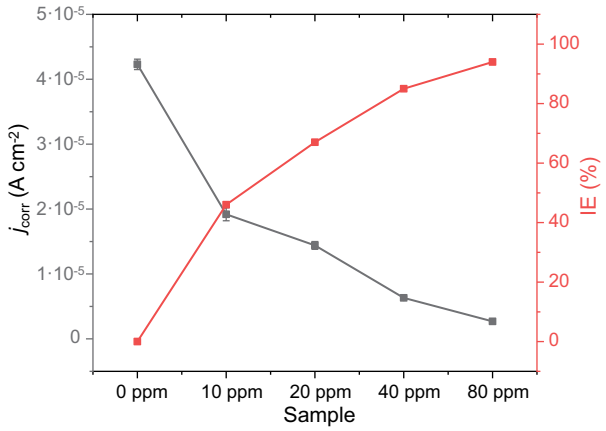


Fig. 3. Corrosion current density i_{corr} and inhibitor efficiency for ASTM A106 Grade B steel in saline water at 55 °C with and without adding nano-silicate inhibitor

a near zero phase shift at low and high frequencies, whereas it peaks at intermediate frequencies as the imaginary component of the impedance increases.

Nyquist plots are mainly represented by a single capacitive loop, indicating that the corrosion of all tested specimens is primarily controlled by the charge transfer process [15]. At low frequencies, however, an inductive loop can be observed in 10 and 20 ppm inhibitor specimens. Increasing the concentration of the inhibitor to 40 ppm resulted in the appearance of a Warburg diffusion element tail with less than 45° slope. Furthermore, at 80 ppm inhibitor concentration, neither inductive loop nor diffusion tail is observed. The semicircle size increases with increasing the concentration of the inhibitor showing the enhancement in the surface charge transfer resistance.

EIS investigation

Fig. 4 and Fig. 5 show the EIS spectrum for all tested specimens in Nyquist and Bode plot format, respectively. Nyquist plots reveal a semicircle with the centre depressed below the *x*-axis, which indicates a non-perfect capacitive behaviour for the surface layer. At high frequencies, the semicircles intersect the *x*-axis, resulting in the solution resistance R_s. When the semicircle intersects the *x*-axis at very low frequencies, it gives the solution resistance plus the total surface resistance (R_s + R_{sl}). At intermediate frequencies, the imaginary part of the impedance begins to increase, indicating a capacitive behaviour. The Bode plot, on the other hand, shows a plateau at high and low frequencies, giving R_s and (R_s + R_{sl}), respectively. In all studied cases, the curve is a straight line with a slope of roughly –1 at intermediate frequencies. Similarly, the phase shift plot shows

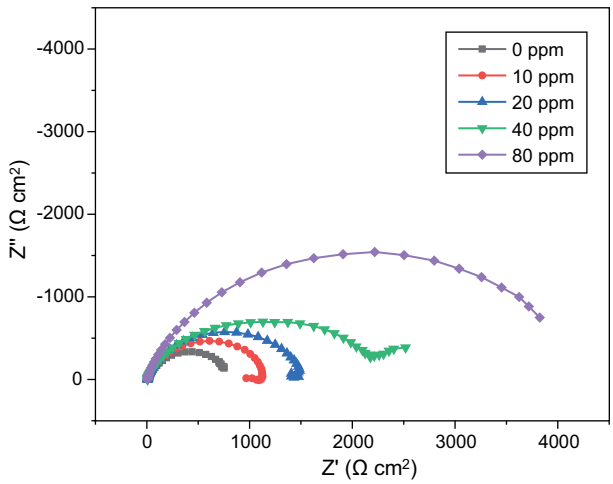


Fig. 4. EIS spectra for ASTM A106 Grade B steel in saline water at 55 °C without and with adding nano-silicate inhibitor in Nyquist format

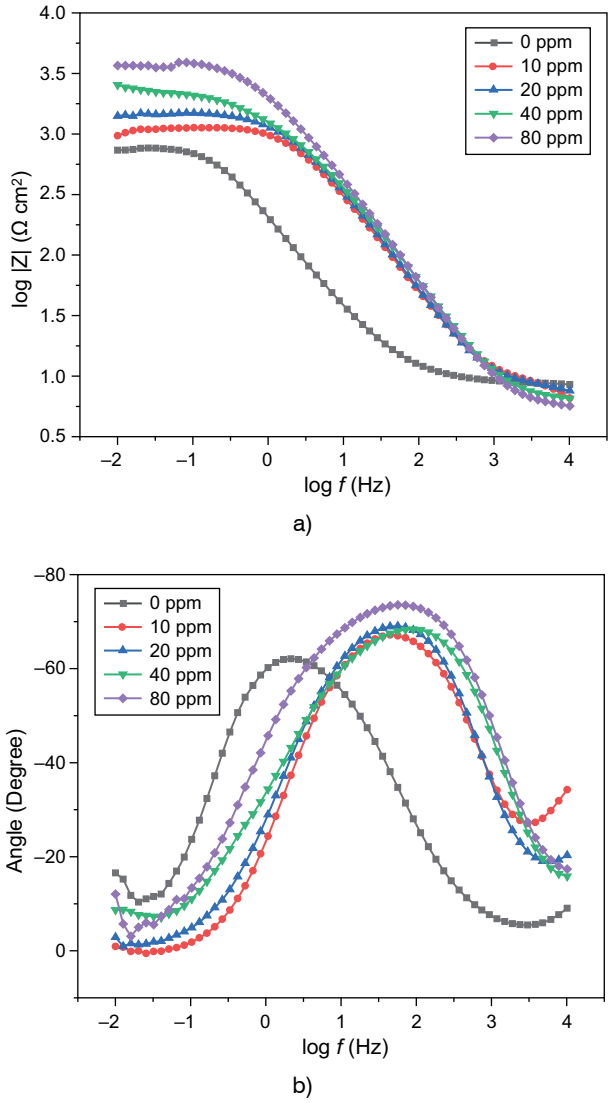


Fig. 5. EIS spectra for ASTM A106 Grade B steel in saline water at 55 °C without and with adding nano-silicate inhibitor in Bode plot format

Phase shift Bode plot (Fig. 5b) reveals changes in the characteristic features of ASTM A106 Grade B steel immersed in saline water at 55°C at high and low frequencies when adding nano-silicate inhibitor. A clear shifting in the phase shift peak toward higher frequencies for all specimens tested in electrolyte with inhibitor compared with free inhibitor electrolyte specimen. Moreover, the phase shift peak angle increases with a higher inhibitor concentration. All these indicate forming an adsorbed layer on the surface and improving the corrosion resistance of the surface by adding a nano-silicate inhibitor.

EIS data was modelled using "Randle's equivalent electric circuit" shown in Fig. 6. This circuit was used because the current work concerns enhancing the corrosion resistance. The inductive loop and the diffusion tail were used as indicators for the surface events, as will be discussed in the discussion section. The circuit is the solution resistance R_s in series with a parallel combination of constant phase element $Q_{SL,}$ and the resistance R_{SL} of the surface layer. The Chi-squared for all the fitting was in the range of 10^{-3} with a fitting error for each element less than 2 %.

All the results of EIS data modelling are tabulated in Tab. 3. R_{SL} increased with adding a nano-silicate inhibitor. The inhibition efficiency IE_{EIS} (%) is determined based on R_{SL} using the following equation:

$$IE_{\text{EIS}}\,\% = \frac{R_{SL}^{\text{inh}} - R_{SL}^{0}}{R_{SL}^{\text{inh}}} \times 100 \qquad (2)$$

where R_{SL}^{inh} and R_{SL}^{0} are the charge transfer resistance after and before adding a nano-silicate inhibitor.

The capacitance value of the surface layer is calculated using the following equation [16], [17]:

$$C^{n} = \frac{R_{SL}^{n-1}}{R_{SL}^{\text{inh}}} \qquad (3)$$

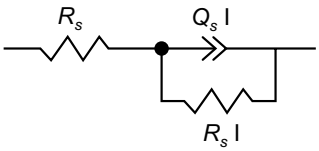


Fig. 6. Equivalent electric circuit EEC used

The capacitance values of all specimens are reported in Tab. 3.

A sharp decrease in the surface capacitance of ASTM A106 Grade B steel immersed in saline water at 55° C was observed when adding the inhibitor to the solution (Fig. 7). The surface capacitance exhibited a plateau over all tested specimens with different concentrations of inhibitor. However, charge transfer resistance continuously increased with higher concentrations of inhibitor.

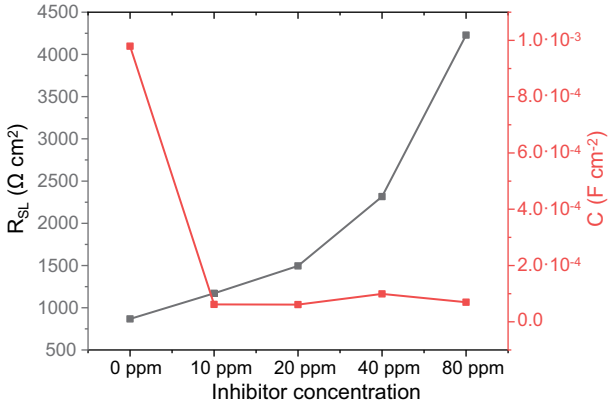


Fig. 7. RSL and C versus inhibitor concentration for ASTM A106 Grade B steel in saline water at 55 °C without and with adding nano-silicate inhibitor

DISCUSSION

Adding nano-silicate inhibitor to saline water resulted in a significant reduction in corrosion rate and high inhibitor efficiency up to 94 % (Tab. 2 and Fig. 3 for ASTM A106 Grade B in saline water at 55°C. The shifting in E_{corr} and OCP toward more noble potentials associated with the noticeable reduction in Tafel cathodic slope β_c (Tab. 2) for all tested specimens indicates that the naturally extracted nano-silicate works as a mixed inhibitor [18]. According to these results, nano-silicate inhibitor reduced anodic dissolution by blocking oxygen from reaching steel surfaces and retarded cathodic reactions via reducing anions diffusion. With high inhibitor concentrations of 40 and 80 ppm, E_{corr} shifted by

Tab. 3 EIS data modling results

Inhibitor concentration	Q_{SL} (F.S$^{\alpha-1}$ cm^{-1}) × 10^{-5}	α_{SL}	R_{SL} (Ω cm^2)	IE_{EIS} (%)	C (F cm^{-2}) × 10^{-5}
0 ppm	101	0.8	867	0	98
10 ppm	9.8	0.82	1171	26	6.18
20 ppm	9	0.83	1495	42	6.13
40 ppm	14.7	0.73	2316	62	9.9
80 ppm	8.8	0.81	4228	79	6.97

more than 85 mV toward anodic potential indicating the predominant anodic effect of the inhibitor at these concentrations [5], [19]. More importantly, using nano-silicate inhibitor successfully reduces the corrosion rate from severe corrosion category to close to low corrosion category for ASTM A106 Grade B in saline water at 55 °C according to NACE standard [20] The dual effect of the inhibitor on the anodic and cathodic reactions is possibly because of forming an adsorbing layer on the surface of ASTM A106 Grade B steel. Surface atoms with unsaturated bonds attract active species from the surrounding gas or liquid media through adsorption. Quite possibly, this phenomenon plays a significant role in corrosion by affecting cathodic reaction, anodic dissolution, or passive film formation. Adsorption of inhibitor on the surface could modify the cathodic reaction by altering the anions availability on the interface. Inhibitor adsorption might also affect the anodic reaction by covering the surface with a compacted adsorbed layer, which partially or totally blocks the cation diffusion.

The capacitance of the surface layer was determined (Fig. 7 and Tab. 3) and found to significantly decrease by ten times from 9.8 μF·cm^{-2} for the free inhibitor specimen to less than 1 μF·cm^{-2} for all specimens with inhibitor. The capacitance value shows a plateau over all tested inhibitor concentrations, which strongly suggests that an adsorbed layer covers the surface. Additionally, the thickness of the surface layer can be associated with the capacitance according to the Helmholtz model [21], [22].

$$C = \varepsilon \cdot \varepsilon_0 \cdot \frac{A}{d} \tag{4}$$

where d denotes the film thickness, A is the active area, ε_0 vacuum permittivity (8.85 × 10^{-14} F·cm^{-1}), and ε is the film dielectric constant. Therefore, the decrease in C when adding the inhibitor to the testing solution can be attributed to the change in dielectric constant (forming the adsorbed layer) and the increase in the thickness of the surface layer. Furthermore, the adsorption of nano-silicate on the ASTM A106 Grade B steel surface in saline water at 55 °C can be described by the adsorption isotherm [23]. The plateau of the capacitance suggests forming a uniform adsorbed surface layer following Langmuir adsorption isotherm [24]. Based on this model, the surface is covered with a single monolayer. It is therefore possible to reach saturation at equilibrium when there is no further adsorption or desorption. In other words, no further adsorption occurs after a certain threshold. To examine the adsorption isotherm, the degree of the surface coverage θ was determined based on the capacitance values extracted from EIS data as follows [25]:

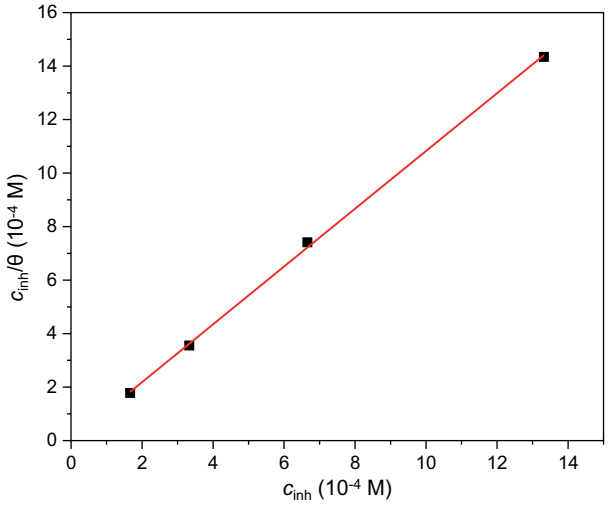


Fig. 8. Langmuir adsorption isotherm plot for ASTM A106 Grade B steel in saline water at 55 °C

$$\theta = \frac{C_{dl}^0 - C_{dl}^i}{C_{dl}^0} \tag{5}$$

where C_{dl} and C_{dl} are the surface capacitance for free inhibitor and with inhibitor specimens, respectively. Langmuir isotherm is given by the following equation [26], [27].

$$\frac{c_{inh}}{\theta} = \frac{1}{K_{ads}} + c_{inh} \tag{6}$$

where c_{inh} is the bulk solution concentration in mol/L, and K_{ads} is the affinity of the adsorbate molecules toward the adsorption surface. Thus, plotting c_{inh}/θ versus c_{inh} should yield a straight line for Langmuir isotherm. A very nice fit is obtained with R^2 equals 0.99 and slope equals unity (Fig. 8), confirming Langmuir adsorption isotherm.

Additionally, the constant K_{ads} is related to the energy of adsorption [28], [29]

$$K_{ads} = \frac{1}{c_{solvent}} \exp\left(\frac{-\Delta G_{ads}}{RT}\right) \tag{7}$$

in which R is the gas constant (8.314 J/mol.K), T is the temperature in K and $c_{solvent}$ is the molar concentration of the solvent, which can be considered here as water (55.56 mol/L). ΔG_{ads} is –46 kJ/mol; such a high value of ΔG_{ads} strongly indicates the occurrence of chemisorption of nano-silicate on the surface of ASTM A106 Grade B steel in saline water at 55 °C.

The appearance of the inductive loop at 10 and 20 ppm inhibitor concentration in the Nyquist plot at low frequencies might be ascribed to the relaxation processes of adsorption of the inhibitor on the surface of ASTM A106 Grade B steel [30], [31]. Increasing the concentration of the inhibitor to 40 ppm resulted in the appearance of a Warburg diffusion element tail with less than 45° slope suggesting forming a porous inhibitor film on the surface [32] and possibly bilayer electrode geometry [33]. Furthermore, at 80 ppm inhibitor concentration, neither inductive loop nor diffusion tail is observed, which indicates the formation of a compacted

adsorbed layer of the nano-silicate on the surface of ASTM A106 Grade B steel. Moreover, it has been shown that as the concentration of the nano-silicate increases in the solution, a more complex distribution is observed by forming dimers, trimers, oligomers, and even higher aggregate [34], [35]. Besides, the presence of polymeric silicate in the silicate solution has been confirmed at high concentration of SiO_2 [36]. Therefore, the appearance of the inductive loop at 10 and 20 ppm nano-silicate specimens, diffusion element at 40 ppm specimen, and disappeared of both of them at 80 ppm specimen (which is associated with continuous increase in the semicircle size with silicate concentration (Fig. 4)) may be attributed to the form of complex aggregates as the nano-silicate concentration increases. These aggregates might physically be adsorbed over the chemically adsorbed monolayer of nano-silicate on the surface of carbon steel as schematically shown in Fig. 10. The chemically adsorbed monolayer of nano-silicate causes a capacitance plateau over all tested inhibitor concentrations (Fig. 8), while the changes in the Nyquist plot EIS spectra (Fig. 5) with inhibitor concentration can be attributed to the physical adsorption of complex aggregate.

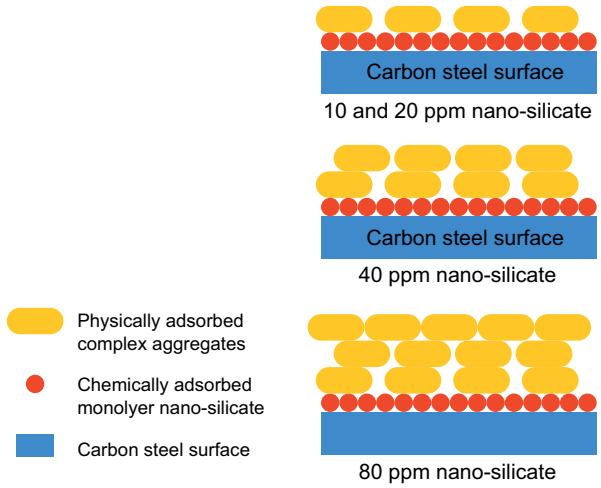


Fig. 9. Nano-silicate aggregates physically adsorbed over chemically adsorbed nano-silicate monolay

CONCLUSIONS

- An abundant agricultural waste was successfully employed to produce green nano-silicate inhibitor.
- With 94 % inhibitor efficiency at 80 ppm inhibitor concentration, the corrosion rate enhanced from 0.94 mm/y (severe corrosion) to 0.031 mm/y (close to low corrosion).
- The inhibition mechanism is forming an adsorbed layer covering the surface from water molecules and chloride ions penetration and blocking the cation diffusion.
- The adsorption process is described using Langmuir adsorption isotherm.
- Increasing the inhibitor's efficiency with a higher concentration of nano-silicate was ascribed to forming complex aggregates of nano-silicate, which might physically be adsorbed over the chemically adsorbed monolayer of nano-silicate on the surface of carbon steel.

REFERENCES

1. Wang C., et al. Modified chitosan-oligosaccharide and sodium silicate as efficient sustainable inhibitor for carbon steel against chloride-induced corrosion, *J Clean Prod*, **2019**, 238, p. 117823.
2. Obot I. B., Onyeachu I. B., Kumar A. M. Sodium alginate: A promising biopolymer for corrosion protection of API X60 high strength carbon steel in saline medium, *Carbohydr Polym*, **2017**, 178, 200–208
3. Awizar D. A., et al. Nanosilicate extraction from rice husk ash as green corrosion inhibitor, *Int J Electrochem Sci*, **2013**, 8, 2, 1759–1769
4. Ji G., et al. Musa paradisica peel extract as green corrosion inhibitor for mild steel in HCl solution, *Corros Sci*, **2015**, 90, 107–117
5. Asra D., Othman N. K., Dasuki Z., Nano-silicate inhibitor derived from rice husk for corrosion mitigation of steel in distilled water, in *AIP Conference Proceedings*, **2017**, 1838, 1, p. 020004
6. Madlangbayan M. S., et al. Corrosion inhibition of sodium silicate with nanosilica as coating in pre-corroded steel, *Civil Engineering Journal (Iran)*, **2021**, 7, 11, 1806–1816
7. Patel K. G., Shettigar R. R., Misra N. M., Recent Advance in Silica Production Technologies from Agricultural Waste Stream–Review" *Journal of Advanced Agricultural Technologies*, **2017**, 4, 3, 274–279
8. Singh S. P. and Endley N. Fabrication of nano-silica from agricultural residue and their application, *Nanomaterials for Agriculture and Forestry Applications*, **2020**, 107–134.
9. Othman N., et al. *Anticorrosive properties of nano silicate from paddy husk in salt medium*, **2016**, Accessed: Feb. 04, 2023. Online.. Available: https://core.ac.uk/download/pdf/84306697.pdf.
10. Asra Awizar D., et al. The Performance of Nanosilicate from Rice Husk Ash as Green Corrosion Inhibitor for Carbon Steel in 0.5M HCl, *Materials Science Forum*, **2013**, 756, 266–272
11. Ajeel S. A., Sukkar K. A., Zedin N. K. Evaluation of acid leaching process and calcination temperature on the silica extraction efficiency from the sustainable sources, *Journal of Physics: Conference Series*, **2021**, 1773, 1, p. 012014
12. Zedin N. K., Ajeel S. A., Sukkar K. A., Nanosilicon powder extraction as a sustainable source (from Iraqi rice husks) by hydrothermal process, *AIP Conference Proceedings*, **2020**, 2213, 1, p. 020155
13. Tao Z., et al. Corrosion inhibition of mild steel in acidic solution by some oxo-triazole derivatives, *Corros Sci*, **2009**, 51, 11, 2588–2595

14. Ashassi-Sorkhabi H., Majidi M. R., Seyyedi K. Investigation of inhibition effect of some amino acids against steel corrosion in HCl solution, *Appl Surf Sci*, **2004**, 225, 1–4, 176–185
15. Behpour M., et al. Investigation of some Schiff base compounds containing disulfide bond as HCl corrosion inhibitors for mild steel, *Corros Sci*, **2010**, 52, 12, 4046–4057
16. Valero Vidal C. and Igual Muñoz A. Study of the adsorption process of bovine serum albumin on passivated surfaces of CoCrMo biomedical alloy, *Electrochim Acta*, **2010**, 55, 28, 8445–8452
17. Cosman N. P., Fatih K., Roscoe S. G. Electrochemical impedance spectroscopy study of the adsorption behaviour of α-lactalbumin and *β*-casein at stainless steel, *Journal of Electroanalytical Chemistry*, **2005**, 574, 2, 261–271
18. Tamalmani K. and Husin H., "Review on corrosion inhibitors for oil and gas corrosion issues," *Applied Sciences*, **2020**, 10, 10
19. Hamdy A. S., Alfosail F., Gasem Z. Eco-friendly, cost-effective silica-based protective coating for an A6092/SiC/17.5p aluminum metal matrix composite, *Electrochim Acta*, **2013**, 89, 749–755
20. "NACE RP0775 - Preparation, Installation, Analysis, and Interpretation of Corrosion Coupons in Oilfield Operations |Engineering360." https://store.ampp.org/sp0775-2013-formerly-rp0775-2 (accessed Jan. 20, 2023).
21. Namus R. and Rainforth W. M. The influence of cathodic potentials on the surface oxide layer status and tribocorrosion behaviour of Ti_6Al_4V and CoCrMo alloys in simulated body fluid, *Biotribology*, 2022, 30, 00212
22. Namus R., et al. The influence of protein concentration, temperature and cathodic polarization on the surface status of CoCrMo biomedical grade alloys, *Appl Surf Sci*, **2020**, 499, 143908
23. Satapathy A. K., et al. Corrosion inhibition by Justicia gendarussa plant extract in hydrochloric acid solution, *Corros Sci*, **2009**, 51, 12, 2848–2856
24. Valero Vidal C. and Igual Muñoz A. Influence of protein adsorption on corrosion of biomedical alloys, *Bio-Tribocorrosion in Biomaterials and Medical Implants*, Elsevier, **2013,** 187–219.
25. Khaled K. F. and Hackerman N. Investigation of the inhibitive effect of ortho-substituted anilines on corrosion of iron in 1 M HCl solutions, *Electrochim Acta*, **2003**, 48, 19, 2715–2723
26. Li X., Deng S., Fu H. Allyl thiourea as a corrosion inhibitor for cold rolled steel in H_3PO_4 solution, *Corros Sci*, **2012**, 55, 280–288
27. Deyab M. A., et al. Experimental evaluation of new inorganic phosphites as corrosion inhibitors for carbon steel in saline water from oil source wells, *Desalination*, **2016**, 383, 38–45
28. Jackson D. R., Omanovic S., Roscoe S. G. Electrochemical studies of the adsorption behavior of serum proteins on titanium, *Langmuir*, **2000**, 16, 12, 5449–5457
29. Valero Vidal C., Olmo Juan A., Igual Muñoz A. Adsorption of bovine serum albumin on CoCrMo surface: Effect of temperature and protein concentration, *Colloids Surf B Biointerfaces*, **2010**, 80, 1, 1–11
30. Singh A. K. and Quraishi M. A. Effect of Cefazolin on the corrosion of mild steel in HCl solution, *Corros Sci*, **2010**, 52, 1, 152–160
31. Deng S. and Li X. Inhibition by Ginkgo leaves extract of the corrosion of steel in HCl and H_2SO_4 solutions, *Corros Sci*, **2012**, 55, 407–415
32. Chen Y. and Jepson W. P. EIS measurement for corrosion monitoring under multiphase flow conditions, *Electrochim Acta*, **1999**, 44, 24, 4453–4464
33. Lee W. J. Inhibiting effects of imidazole on copper corrosion in 1 M HNO_3 solution, *Materials Science and Engineering A*, **2003**, 348, 217–226
34. Yang X., Roonasi P., Holmgren A. A study of sodium silicate in aqueous solution and sorbed by synthetic magnetite using in situ ATR-FTIR spectroscopy, *J Colloid Interface Sci*, **2008**, 328, 1, 41–47
35. Gao H., et al. Study of the corrosion inhibition effect of sodium silicate on AZ91D magnesium alloy, *Corros Sci*, **2011**, 53, 4, 1401–1407
36. Bass J. L. and Turner G. L. Anion distributions in sodium silicate solutions. Characterization by 29SI NMR and infrared spectroscopies, and vapor phase osmometry, *Journal of Physical Chemistry B*, **1997**, 101, 50, 10638–10644